J. Fluid Mech. (1978), *vol.* 88, *part* 1, *pp.* 133–160
Printed in Great Britain

Intermittency and preferential transport of heat in a round jet

By R. CHEVRAY AND N. K. TUTU†
Department of Mechanical Engineering, State University of New York, Stony Brook

(Received 24 January 1977 and in revised form 5 December 1977)

The temperature and velocity fields in a round heated jet were investigated in detail. Both conventional measurements and conditional measurements (zone averages and point averages) were performed. The probability density functions of the lengths of turbulent and non-turbulent durations were also measured. Filtered correlation measurements show that large-scale turbulent motions were responsible for the bulk of momentum and heat transport, and also that small scales were more efficient in transporting heat than in transporting momentum. In no case was heat transported further or more than momentum, however. These results are discussed in detail, particularly with regard to the entrainment. Conservation equations for turbulent-zone variables and the intermittency factor are derived and a model for some of the resulting higher-order correlations is suggested. An exact equation for the intermittency function is presented.

1. Introduction

Free turbulent shear flows have been the subject of considerable experimental investigation in the past. The axisymmetric jet, in particular, was investigated as early as 1943 by Corrsin, in 1949 by Hinze & Van der Hegge Zijnen and later in more detail by Corrsin & Uberoi (1950). Although these experiments have clearly established the preferential lateral transport of scalar quantities like heat over vector quantities like momentum, as translated into the inequalities which hold between the eddy diffusivities for momentum and heat, no light has been thrown upon the possible differences in the transport mechanisms. From the discovery of intermittency in free turbulent shear flows by Corrsin (1943) and one of the first comprehensive studies of this phenomenon, by Corrsin & Kistler (1954), it has been recognized that intermittency plays a dominant role in such flows. On the one hand, this double statistical structure requires that in detailed studies measurements be made either separately in turbulent and non-turbulent zones (conditional zone averages) or with respect to the interface location (conditional point averages). On another hand, to investigate the differences in the transfer mechanisms of heat and momentum, filtered correlation measurements $\overline{u_f v_f}$ and $\overline{v_f \theta_f}$ need to be made. These measurements obviously require simultaneous and continuous signals for the velocity components and temperature; techniques to obtain them were developed and used here. Finally, with a view to

† Present address: Department of Aeronautical Engineering Sciences, University of Colorado, Boulder, Colorado 80302.

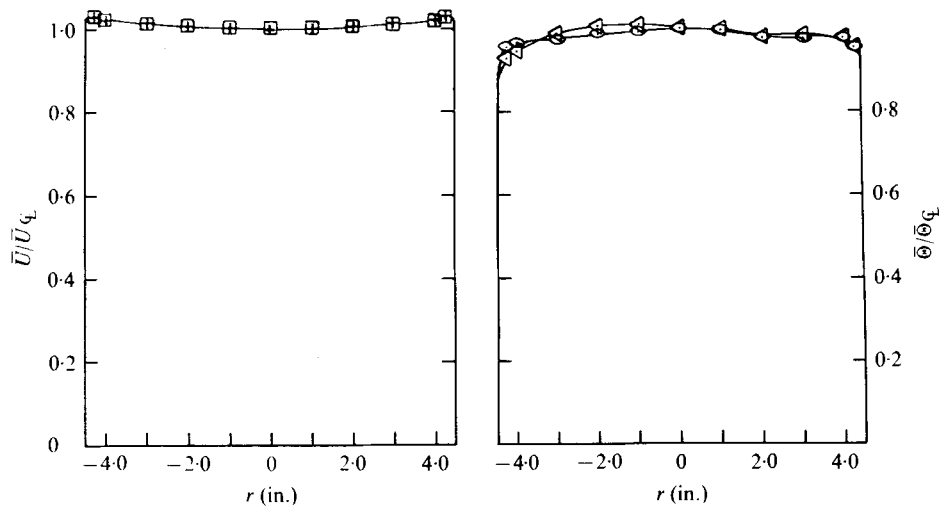

FIGURE 1. Longitudinal velocity and temperature profiles at jet exit.
□, ⊙, vertical; +, ◁, horizontal.

describing and predicting these and similar flows more readily, equations for conditionally averaged variables are presented.

2. Flow facility and experimental techniques

The heated jet facility consists mainly of an airfoil blade fan driven by a 7·5 h.p. d.c. motor equipped with an SCR speed control. This discharges through a bank of 15 finned heaters (22·5 kW) into a diffuser whose end cross-section is circular. After passing through a settling chamber equipped with screens, a honeycomb and a 16 : 1 contraction, the axisymmetric circular jet emerges with a diameter D of 22·5 cm into the room from the centre of a flat circular plate 124 cm in diameter. From the diffuser onwards, the jet facility is insulated throughout and to produce as rectangular as possible an exit temperature profile (figure 1) a collar heater (which circulates air at the same temperature as that of the jet) is provided at the end of the contraction. In order to detect readily any buoyancy effect, the whole unit was installed horizontally. At 15 diameters downstream, where both horizontal and vertical profiles were measured, no marked departure from symmetry was observed. Nominal values of the mean velocity and temperature (above ambient) at the jet exit were 25 m/s and 20 °C, respectively, while the turbulence intensity was measured to be a little less than 0·5 %. This results in a value of $0{\cdot}23 \times 10^{-3}$ for the ratio $gL\Delta\Theta/(\Theta\bar{U}^2)$ of buoyant forces to inertia forces, showing that the temperature can be treated here as a dynamically passive scalar field. Previous measurements by Chevray & Tutu (1972) in the same jet facility and with the same exit conditions demonstrated the virtual identity of velocity spectra for the heated (non-isothermal) and isothermal jets.

To permit simultaneous measurements of temperature and velocity, a special instrument was developed for this study and has been reported on earlier by Chevray & Tutu (1972). Essentially, it consists of two hot-wire probes, one of which operates

in the low-overheat constant-current mode, thus providing a signal directly proportional to the temperature, whereas the other operates in the constant-temperature mode, providing a signal with contributions from both the temperature and the velocity. Information on the velocity field alone was thus obtained from this second hot wire by generating the proper function of temperature given by the first and conditioning the signal through an analog circuit. Dynamic compensation was provided so that a linear signal representative of the velocity field alone was obtained. This technique was adapted to a cross-wire configuration, thus permitting direct measurements of not only the shear stress and heat transfer but also filtered correlations between velocity and temperature.

Measurements with inclined wires are based on the response equation

$$U_{\text{eff}} = \{U_{\text{nor}}^2 + k^2 U_{\text{ax}}^2\}^{\frac{1}{2}}, \tag{1}$$

where U_{eff} is the instantaneous effective cooling velocity, U_{nor} and U_{ax} are the components of the velocity vector normal and parallel to the hot wire, respectively, and k is the axial sensitivity. In high intensity turbulent flows, besides the axial sensitivity k and the sensitivity to the w component of velocity, rectification is an additional source of error in conventional measurements with cross-wires. Champagne & Sleicher (1967) have demonstrated that the error in second-order moments due to k is negative and Tutu & Chevray (1975) have shown that the errors due to the other two causes (independently) are of the same sign. Shear-stress measurements have been corrected for the former errors.

For all the measurements, two hot-wire probes were used. When only the longitudinal velocity component and the temperature were needed, a standard DISA 55A39 hot-wire probe was used with its stem parallel to the flow direction. This probe has two mutually orthogonal hot-wire sensors that are perpendicular to the probe axis. For simultaneous measurements involving quantities other than those mentioned above, a standard cross-wire 55A32 was used with the temperature sensor located upstream from and perpendicular to both cross-wires. In the constant-temperature mode, all sensors were 3·8 μm diameter tungsten wires spot welded to the prongs. For temperature measurements, the sensor was etched from a spot-welded Wollaston wire (10 % Rh, 90 % Pt) of diameter 0·635 μm. This wire was operated in the constant-current mode with a sensor current of 0·15 mA using a Flow Corporation 1900-1 constant-current anemometer, thus acting as a simple resistance thermometer. The sensitivity of direct measurement of the velocity was found to be 0·009 °C(m/s)$^{-1}$. At zero flow velocity the frequency response was good up to (3 dB down) 5·7 kHz and this increased to 10·7 kHz at a flow velocity of 5 m/s.

Throughout this investigation, d.c. coupling has been used for all measurements. Although this renders measurements more tedious it is well worth the advantage of eliminating the distortion in signals due to low frequency loss encountered in a.c. coupling. Most measurements were made digitally using Hewlett–Packard 2212A voltage-to-frequency (100000 (pulses/s) V^{-1}) converters and modified (with seven digits and a 100 s gate time) Hewlett–Packard 5330A preset counters to perform a true integration. To minimize scatter, long integration times (5 min) were used. For measurements of odd moments and cross-correlations a d.c. electronic splitter was built in order to separate the signal into positive and negative parts for simultaneous integration.

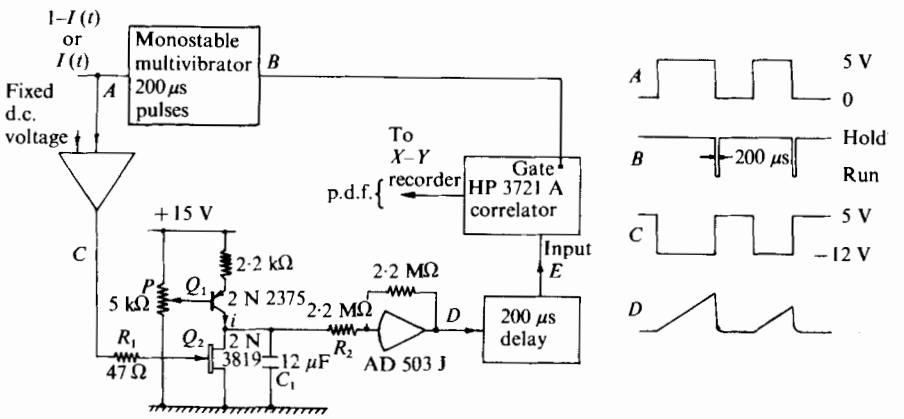

FIGURE 2. Measurement of the p.d.f. of turbulent and non-turbulent durations.

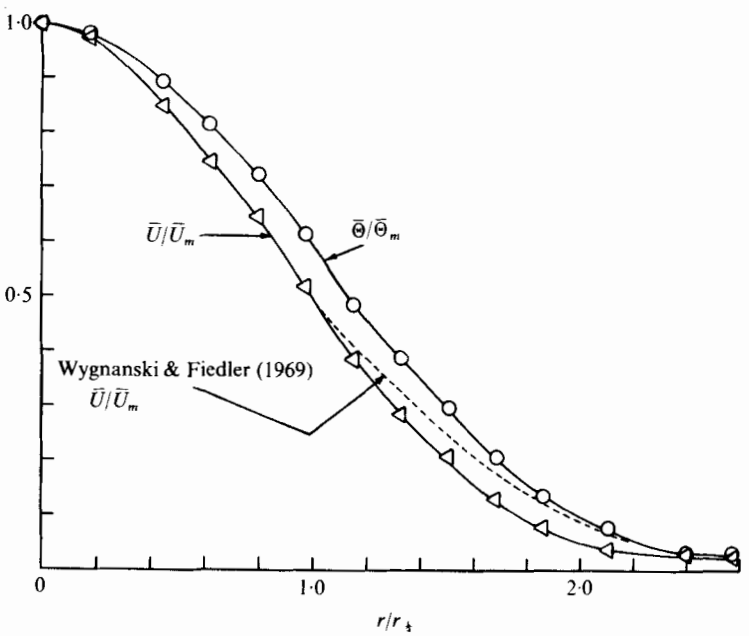

FIGURE 3. Longitudinal velocity and temperature profiles.
$x/D = 15$, $r_{\frac{1}{2}} = 11{\cdot}3$ in., $\bar{U}_m = 11{\cdot}83$ m/s, $\bar{\Theta}_m = 7{\cdot}55$ °C.

Several general-purpose electronic instruments were used throughout this study. More specialized ones were a PAR TDH-9 wave-form eductor, a PAR CW-1 boxcar integrator, an HP 3271A correlator, and a Holeywell 7610 FM tape recorder equipped with phase lock. For the measurement of the probability density function (p.d.f.) of the lengths of turbulent and non-turbulent durations a special circuit was built to convert the intermittency signal (a random square wave) to a random sawtooth wave, the peak of the sawtooth being proportional to the length of the turbulent or non-turbulent duration. By giving an appropriate triggering pulse to the HP 3721A correlator, it was possible to take a single sample of the voltage of the sawtooth wave form each time it reached its peak and thus obtain the required p.d.f. Figure 2 shows the circuit diagram together with a schematic diagram of the measurement procedure.

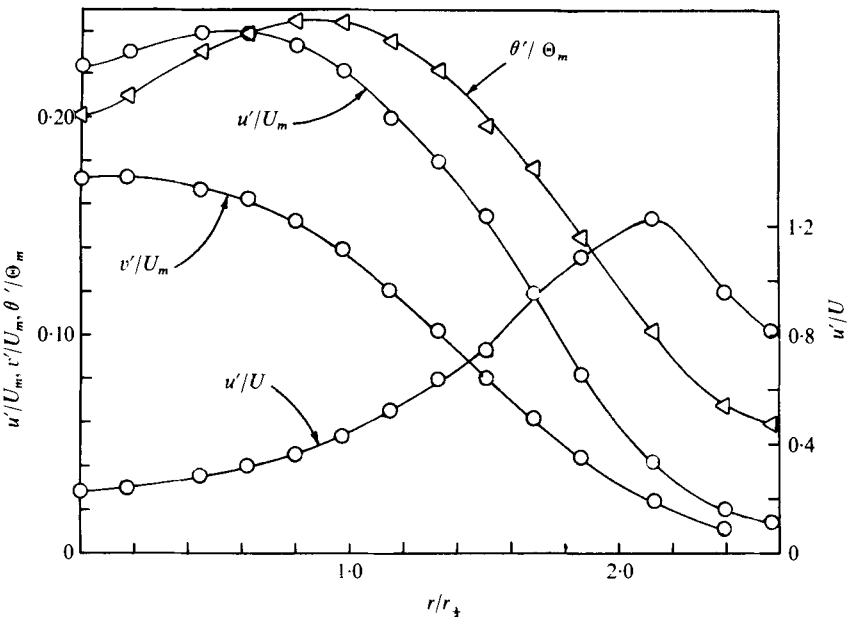

FIGURE 4. Velocity and temperature fluctuations at $x/D = 15$.

3. Gross characteristics: conventional, point and zone averages

All the measurements were performed at $x/D = 15$; this choice was dictated more by experimental constraints than by any theoretical considerations. While Wygnanski & Fiedler's (1969) measurements in an isothermal round jet clearly show that complete dynamical similarity is reached only about 70 diameters downstream of the jet exit, at such large x/D values a much larger exit temperature difference would be needed to permit temperature measurements to be made. This would obviously conflict directly with our requirement that the temperature field be dynamically passive. Figure 3 shows the mean longitudinal velocity and temperature profiles together with the measurements made by Wygnanski & Fiedler (1969) in the self-preserving region. This relatively flatter distribution of temperature as compared with the mean velocity is associated with the preferential transport of heat over momentum. It must be mentioned here that the temperature profile has been corrected for the contamination due to the influence of the velocity-sensing hot wire. This was done by measuring the mean temperature profiles with the velocity-sensing hot wire on and off. The corrections were significant only for $r/r_{\frac{1}{2}} > 1{\cdot}65$.

Velocity and temperature fluctuation intensities are presented in figure 4. The relatively large value of the temperature fluctuations at the tail of the jet is due to fluctuations in the ambient temperature. Had we used a.c. coupling (with a cut-off at 0·5 Hz, say) these very low frequency ambient temperature fluctuations would have been filtered out, and thus might have remained unnoticed. Again, in the outer regions of the jet the θ' profile was obtained by switching the velocity-sensing wire off. In agreement with Wygnanski & Fiedler's (1969) measurements, v' is everywhere less than u'.

To distinguish between the turbulent and non-turbulent states we must monitor a property of the flow which shows a marked difference across the turbulent/non-

turbulent interface. An ideal detector probe would then be a vorticity probe giving us a continuous signal proportional to a component of the vorticity. Contrary to what is generally thought, a two-wire probe sensitive to $\partial U/\partial y$ is not a good substitute for a vorticity probe, because although in the turbulent region $\partial\tilde{\tilde{U}}/\partial y \gg \partial\tilde{\tilde{V}}/\partial x$, in the non-turbulent region $\partial\tilde{\tilde{U}}/\partial y = \partial\tilde{\tilde{V}}/\partial x$. Besides, and more important, instantaneous values $\partial U/\partial y$ and $\partial V/\partial x$ are of the same order, so even in the turbulent region $\partial U/\partial y$ is not a good approximation for the vorticity component. For simplicity, therefore, it was decided to use $\partial u/\partial t$ as the basic signal from which to generate the intermittency function. Since the velocity fluctuations in the non-turbulent region are of a much lower frequency than the fluctuations in the turbulent zone, and since differentiation is nothing but selective amplification of high frequency components, $\partial u/\partial t$ should provide a good contrast between the turbulent and non-turbulent states. Moreover, assuming isotropy and Taylor's hypothesis, $\partial u/\partial t$ can also be visualized as being proportional to the square root of turbulent energy dissipation; thus reasonably good detection can be expected from it.

Since the turbulence detector was designed and built (Chevray & Tutu 1972), many other turbulence detection schemes have appeared in the literature (e.g. Thomas 1973; Paizis & Schwarz 1974). The approach used here is described by Tutu (1976) and is basically the same as that used by Kibens (1968). The actual circuit design, however, has been improved; in particular, the so-called 'hold time stage' (smoothing circuit) works on a completely different principle and is free of the defects and limitations of the previous hold time stage described by Tutu & Chevray (1976).

We denote by γ the temporal mean of the intermittency function I. Its 'frequency' f_γ is half the interface crossing rate. Let $Q(\mathbf{x}, t)$ be a fluid-mechanical property, then its conventional average $\bar{Q}(\mathbf{x})$, its turbulent zone average $\bar{Q}_t(\mathbf{x}) = \tilde{\bar{Q}}$ and its non-turbulent zone average $\bar{Q}_n(\mathbf{x}) = \tilde{\tilde{Q}}$ are defined by

$$\begin{aligned}
\bar{Q}_t(\mathbf{x}) &= \lim_{T\to\infty}\left\{\int_{t_0}^{t_0+T} Q(\mathbf{x},t)\,I(\mathbf{x},t)\,dt \Big/ \int_{t_0}^{t_0+T} I(\mathbf{x},t)\,dt\right\} \\
&= \overline{QI}/\bar{I} = \tilde{\bar{Q}}, \\
\bar{Q}_n(\mathbf{x}) &= \lim_{T\to\infty}\left\{\int_{t_0}^{t_0+T} Q(\mathbf{x},t)\,[1-I(\mathbf{x},t)]\,dt \Big/ \int_{t_0}^{t_0+T} [1-I(\mathbf{x},t)]\,dt\right\} \\
&= \overline{Q(1-I)}/\overline{(1-I)} = (\bar{Q}-\gamma\bar{Q}_t)/(1-\gamma) = \tilde{\tilde{Q}}, \\
\bar{Q}(\mathbf{x}) &= \lim_{T\to\infty}\left\{\int_{t_0}^{t_0+T} Q(\mathbf{x},t)\,dt \Big/ \int_{t_0}^{t_0+T} dt\right\} = \bar{Q}.
\end{aligned}$$

From these three kinds of average, three kinds of fluctuation arise:

$$q = Q-\bar{Q}, \quad q_t = Q-\bar{Q}_t, \quad q_n = Q-\bar{Q}_n.$$

If $P(\mathbf{x}, t)$ is another fluid-mechanical property, then three kinds of cross-correlation suggest themselves:

$$\begin{aligned}
\overline{pq} &= \overline{(P-\bar{P})(Q-\bar{Q})}, \quad \widetilde{\overline{p_t q_t}} = \overline{(P-\bar{P}_t)(Q-\bar{Q}_t)\,I}/\bar{I}, \\
\widetilde{\overline{p_n q_n}} &= \overline{(P-\bar{P}_n)(Q-\bar{Q}_n)\,(1-I)}/\overline{(1-I)},
\end{aligned}$$

where, as it is clear, $(-)$ denotes the conventional average, $(\tilde{\ })$ denotes the turbulent

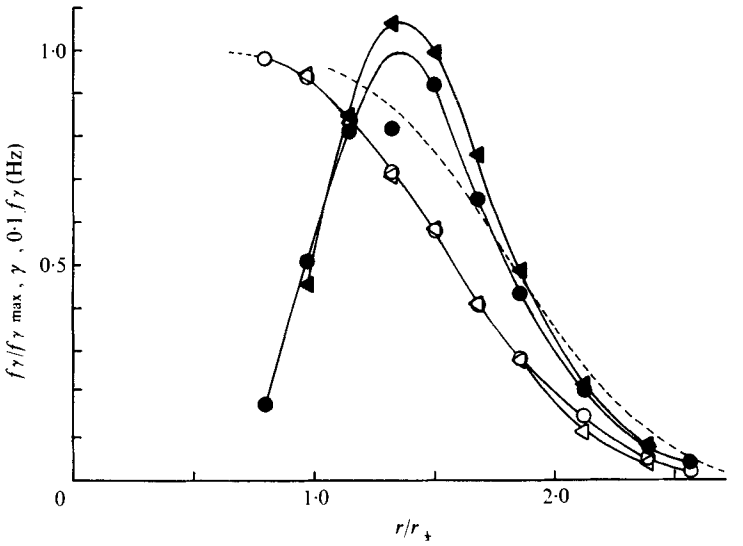

FIGURE 5. Distribution of γ and f_γ across the jet. – – –, γ in the similarity region (Corrsin & Kistler 1954); ○, ●, γ and $f_\gamma/f_{\gamma\max}$ at $x/D = 15$ (from single wire); ◁, ◀, γ and $f_\gamma/f_{\gamma\max}$ at $x/D = 15$ (from X-wire).

zone average and ($\simeq$) denotes the non-turbulent zone average. The following relations are then easily proved:

$$\overline{Q} = \gamma\overline{Q}_t + (1-\gamma)\,\overline{Q}_n,$$
$$\overline{pq} = \gamma\widetilde{\overline{p_t q_t}} + (1-\gamma)\widetilde{\overline{p_n q_n}} + \gamma(1-\gamma)\{\overline{P}_t\,\overline{Q}_t + \overline{P}_n\,\overline{Q}_n - \overline{P}_t\,\overline{Q}_n - \overline{P}_n\,\overline{Q}_t\},$$
$$\overline{q^2} = \gamma\widetilde{\overline{q_t^2}} + (1-\gamma)\widetilde{\overline{q_n^2}} + (1-\gamma)\{\overline{Q}_t - \overline{Q}_n\}^2.$$

The 'switching terms' in the braces arise from the change in mean level from turbulent to non-turbulent regions. Let

$$\hat{p}(\mathbf{x},t) = \tfrac{1}{2}(\dot{I}(\mathbf{x},t) + |\dot{I}(\mathbf{x},t)|), \quad \check{p}(\mathbf{x},t) = \tfrac{1}{2}(|\dot{I}(\mathbf{x},t)| - \dot{I}(\mathbf{x},t)),$$

where $\dot{I}$ is the time derivative of I. $\hat{p}(t)$ is then a series of positive-travelling δ-functions with each pulse occurring at the leading edge (downstream crossing, where the intermittency function changes from zero to unity) and $\check{p}(t)$ is a pulse train with each pulse occurring at the trailing edge (upstream crossing, where $I(t)$ changes from unity to zero). These functions are used to define the leading-edge point average $\hat{Q}$ of Q and the trailing-edge point average $\check{Q}$ of Q as

$$\hat{Q}(\mathbf{x}) = \lim_{T\to\infty}\left\{\int_{t_0}^{t_0+T} Q(\mathbf{x},t)\,\hat{p}(\mathbf{x},t)\,dt \Big/ \int_{t_0}^{t_0+T} \hat{p}(\mathbf{x},t)\,dt\right\} = \overline{Q\hat{p}}/\overline{\hat{p}} = \overline{Q\hat{p}}/f_\gamma,$$
$$\check{Q}(\mathbf{x}) = \overline{Q\check{p}}/f_\gamma.$$

We can also define a more general type of conditional point average where the detector probe (from which $\hat{p}$ or $\check{p}$ is derived) and the sampling probe (which supplies Q) are separated by a certain distance $\mathbf{r}$ in space and a time lag τ:

$$\hat{Q}(\mathbf{x},\mathbf{r},\tau) = \overline{Q(\mathbf{x}+\mathbf{r},t+\tau)\,\hat{p}(\mathbf{x},t)}/f_\gamma(\mathbf{x}).$$

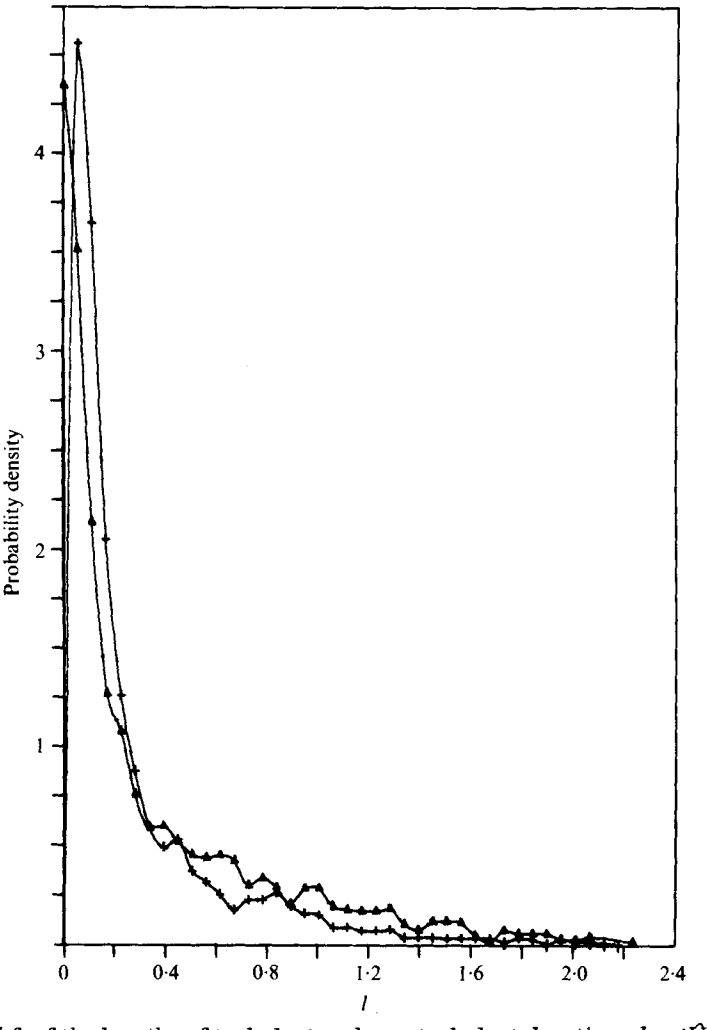

FIGURE 6. P.d.f. of the lengths of turbulent and non-turbulent durations. $l = t\hat{U}/r_{\frac{1}{2}}$, t = duration of turbulent or non-turbulent zone. ▲, turbulent durations, $\bar{l} = 0{\cdot}39$, $\sigma_l = 0{\cdot}45$; +, non-turbulent durations, $\bar{l} = 0{\cdot}28$, $\sigma_l = 0{\cdot}34$. $\gamma = 0{\cdot}58$, $x/D = 15$.

Distributions of the intermittency factor γ, the burst rate f_γ and $f_\gamma/f_{\gamma\max}$ are shown in figure 5. Corresponding measurements by Corrsin & Kistler (1954) in the self-preserving region are also shown for reference. From this figure, it appears that the non-turbulent fluid penetrates relatively deeper in the initial regions than further downstream.

In figures 6 and 7, the times of the turbulent and non-turbulent durations have been non-dimensionalized with $\hat{U}/r_{\frac{1}{2}}$ in order to yield an estimate of the lengths involved. Since the ratio of the standard deviations of these durations to the mean duration is greater than 1 in all the four cases, it is clear that there is nothing like an average bulge. Consequently, it will be quite meaningless to construct an average shape of the bulge from the average lengths γ/f_γ and $(1-\gamma)/f_\gamma$ of turbulent and non-turbulent durations. Since the p.d.f.'s resemble the shape which one would obtain from a

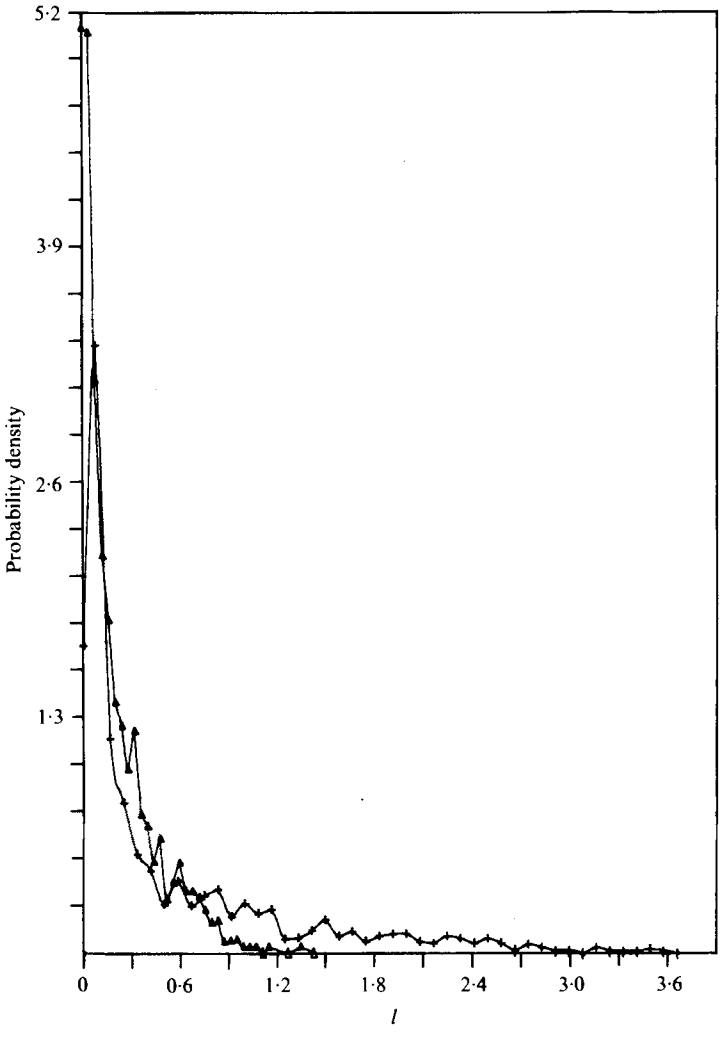

FIGURE 7. P.d.f. of the lengths of turbulent and non-turbulent durations. △, turbulent durations, $\bar{l} = 0{\cdot}21, \sigma_l = 0{\cdot}22$; +, non-turbulent durations, $\bar{l} = 0{\cdot}54, \sigma_l = 0{\cdot}69$. $\gamma = 0{\cdot}28, x/D = 15$.

Poisson model (where the probability of getting a front or a back in the time interval dt is $2f_\gamma\, dt$ and which is independent of the existence of the interface in the immediate past) it is apparent that the interface is a highly convoluted surface which moves in a random manner as was also noticed by Thomas (1973) for the plane turbulent wake.

Figure 8 shows the conditional zone averages of U and Θ across the jet. As expected, the fluid in the turbulent zones is seen to be travelling much faster than the fluid in the non-turbulent zones. The fact that the temperature is non-zero in non-turbulent zones and the gradients of $\overline{\Theta}$ and $\widetilde{\Theta}$ have the same sign is rather curious. Its possible implications will be discussed in §4. Again, in the turbulent zones the temperature distribution is much flatter than U_t, showing that the scalar field is 'mixed' much better than the momentum. Figure 9 shows the fluctuation intensity of the longitudinal component of velocity in the two zones. As a comparison with figure 4 shows, for

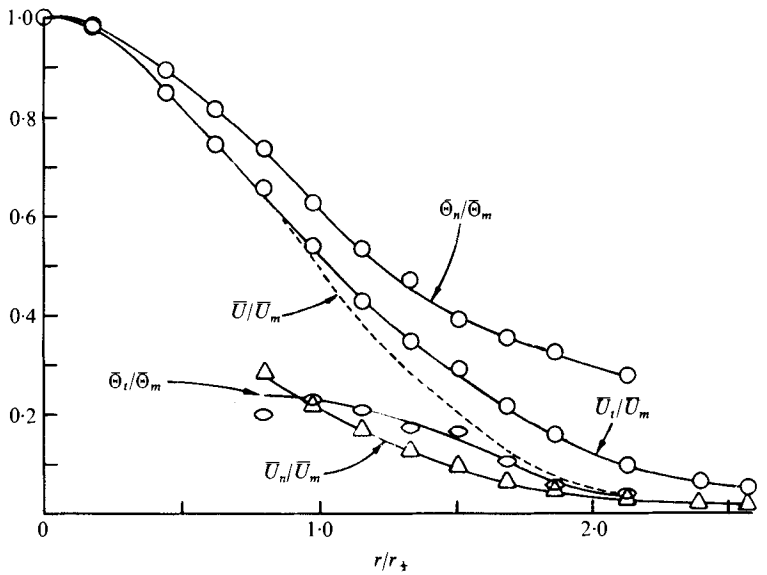

FIGURE 8. Conditional velocity and temperature profiles.

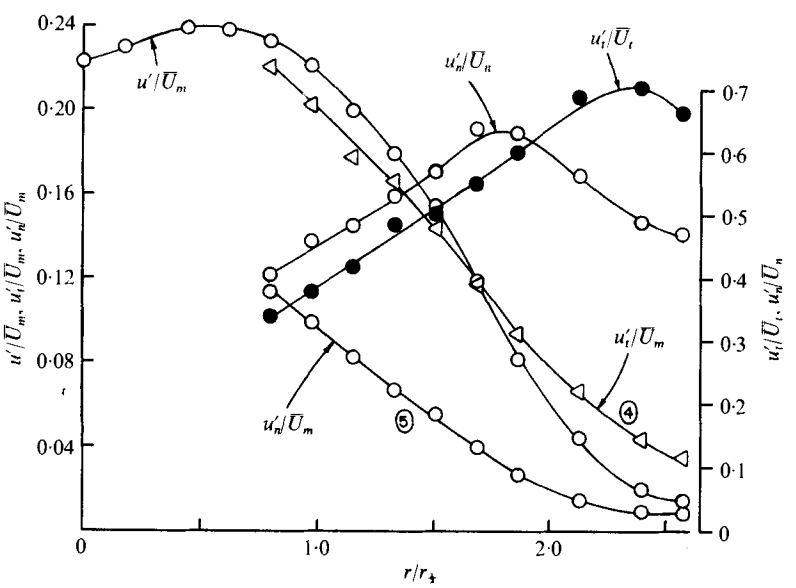

FIGURE 9. Zone-averaged longitudinal velocity fluctuation.

$r/r_{\frac{1}{2}} > 1{\cdot}15$ the local turbulent intensities in the two zones are less than the unconditioned local turbulence intensity. The maximum value of about 0·7 for $u'_t/\overline{U}_t$ is much less than the maximum value of 1·2 for $u'/\overline{U}$, thus showing that the errors due to the assumed simple linearized hot-wire response are not as great as the unconditioned local turbulence intensity would indicate. The conditional averages of the radial component of velocity depicted in figure 10 show that, as expected, the non-turbulent fluid is moving inwards on average while the turbulent fluid is moving outwards. Near the tail of the jet, the relatively large positive values of $\overline{V}_t$ indicate that

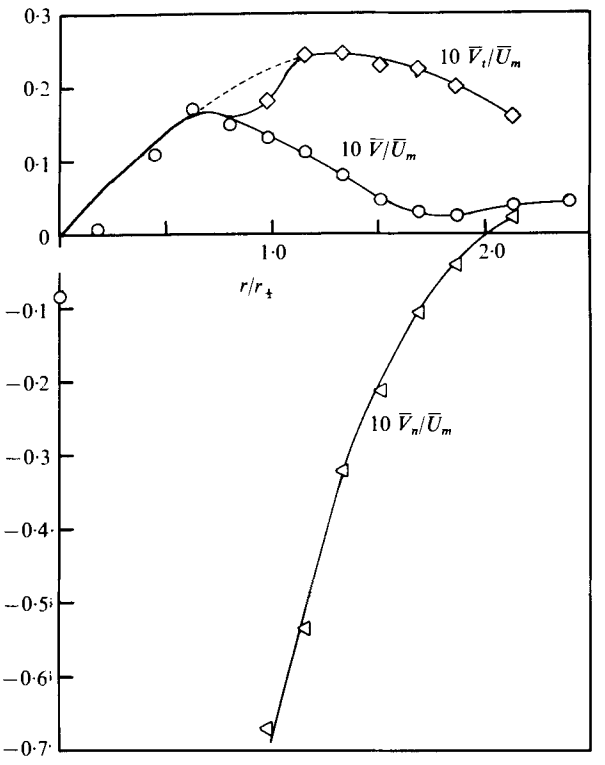

FIGURE 10. Zone-averaged lateral velocity profile.

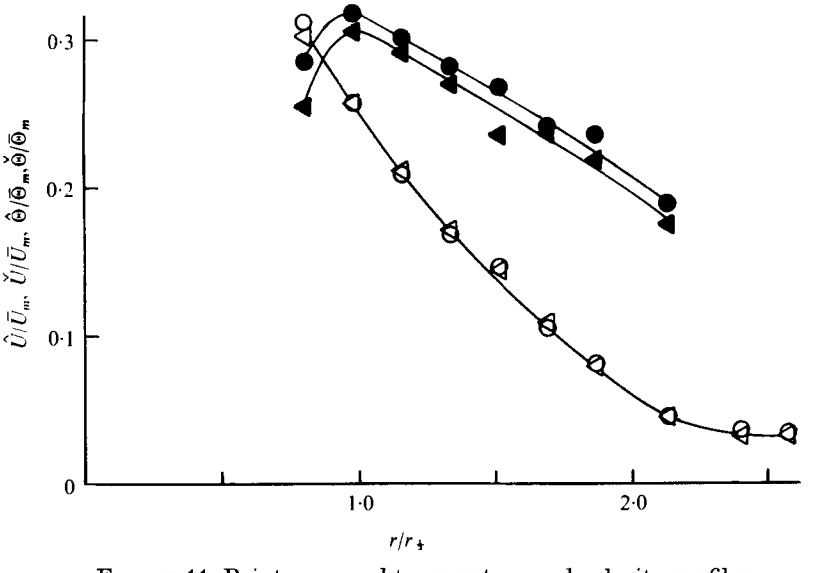

FIGURE 11. Point-averaged temperature and velocity profiles.
○, $\hat{U}/\bar{U}_m$; ◁, $\check{U}/\bar{U}_m$; ●, $\hat{\Theta}/\bar{\Theta}_m$; ◀, $\check{\Theta}/\bar{\Theta}_m$.

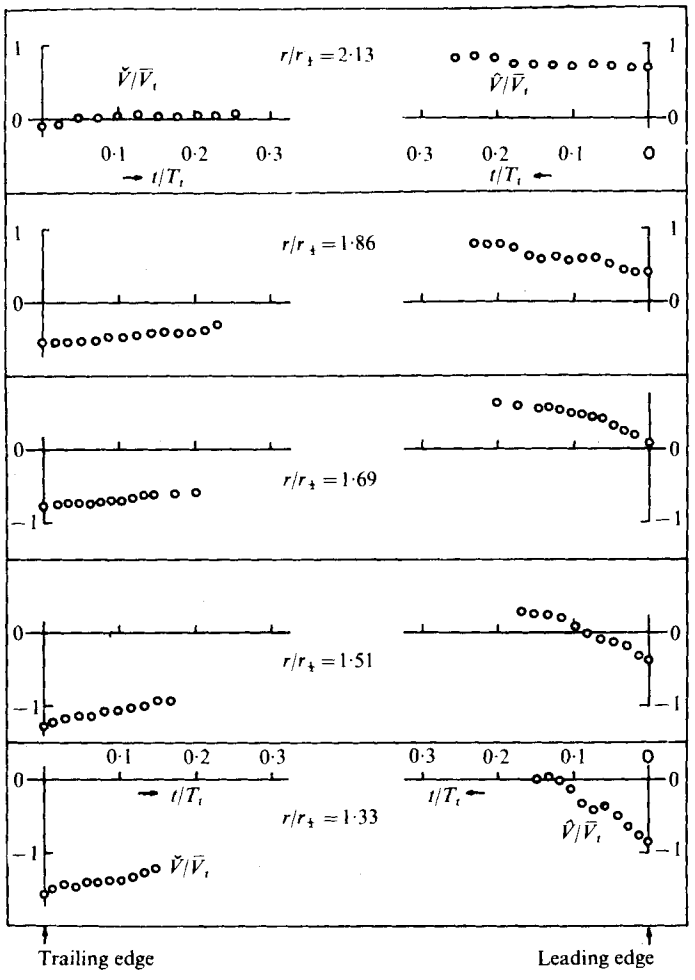

FIGURE 12. Point-averaged lateral velocity distribution inside the turbulent bulge at $x/D = 15$.

once in a while the turbulent bulges shoot out. Similarly, large negative values of $\bar{V}_n$ deep inside the jet show that the non-turbulent fluid is rushing in to be entrained, which suggests that perhaps there are deep crevices in the turbulent/non-turbulent interface in regions of high γ where significant entrainment is taking place. For large radial distances, the strange behaviour of the unconditioned radial velocity $\bar{V}$ comes from the effects of rectification and distortion due to high turbulence intensity.

Leading- as well as trailing-edge velocity (longitudinal component) and temperature profiles are presented in figure 11. They reveal that on average the fluid at the leading edge is travelling with the same longitudinal velocity as that at the trailing edge. That the point-averaged temperature profile is flatter than the point-averaged velocity profile, giving yet more evidence that the temperature field is more homogeneous in the turbulent zones than the velocity field, is as expected. The remarkable feature here, however, is that $\partial\hat{\Theta}/\partial r$ and $\partial\check{\Theta}/\partial r$ are both positive for $\gamma > 0{\cdot}95$. This can be explained only if unusually large entrainment is taking place deep inside the jet in

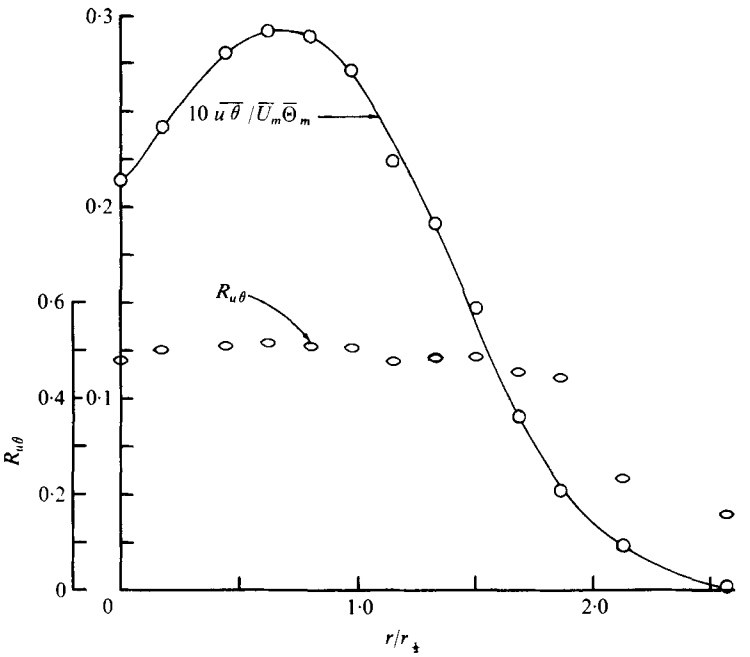

FIGURE 13. Cross-correlation between u and θ.

Flow field	Experiment	σ_t	Author(s)
Planar	Wake of heated cylinder	0·54	Fage & Falkner
Planar	Heated jet	0·54	Reichardt
Planar	Heated jet	0·42–0·59	Van der Hegge Zijnen
Axisymmetric	Heated jet with tracers	0·74	Van der Hegge Zijnen
Axisymmetric	Heated jet	0·76	Ruden
Axisymmetric	Nitrogen jet	0·72	Keagy & Weller
Axisymmetric	Heated jet	0·70	Corrsin
Axisymmetric	Heated jet	0·71	Forstall
Axisymmetric	Submerged water jet	0·72–0·83	Forstall & Gaylord

TABLE 1. σ_t for jets and wakes (Mayer & Divorky 1966).

these regions of high γ, which is consistent with the earlier observation (figure 10) of large negative values of $\overline{V}_n$ in the regions of high γ.

Conditional point measurements with respect to the existence of the interface (at the point) at a certain time t before or after were made. Radial velocities were measured in this way and are plotted in figure 12. They show several interesting features, chief among which is that the radial velocities near the interface behave very differently on the upstream and downstream sides of the interface. For $r/r_{\frac{1}{2}} < 1{\cdot}66$ the fluid near the leading edge is moving inwards, while beyond $r/r_{\frac{1}{2}} = 1{\cdot}66$ it is moving outwards. In contrast, however, the fluid near the trailing edge is on average always moving inwards.

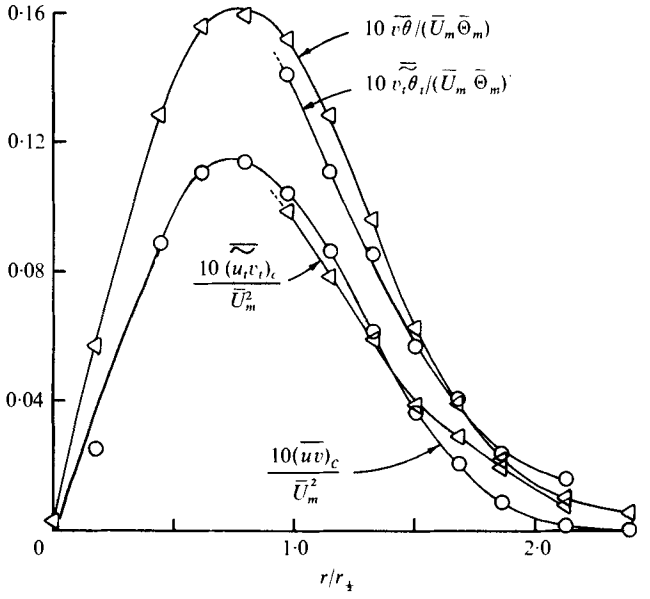

FIGURE 14. Distribution of turbulent shear and heat transfer.

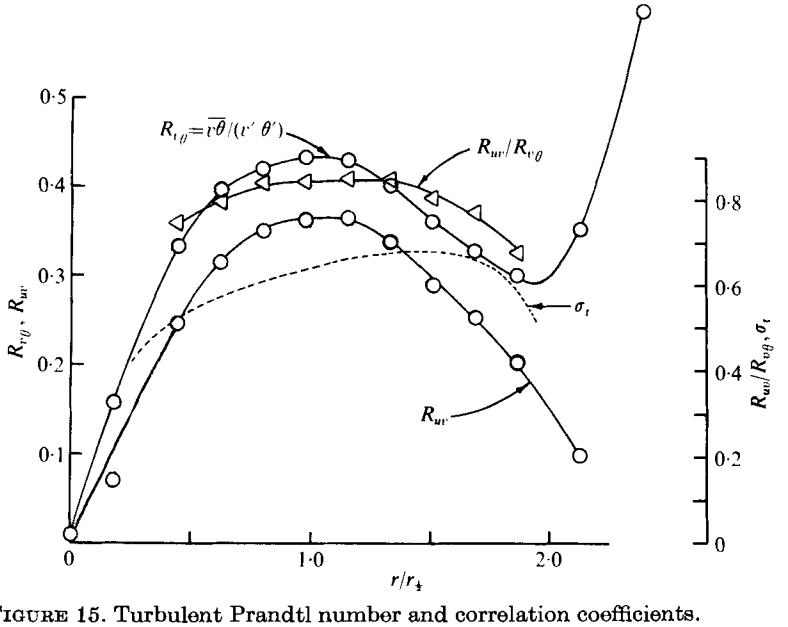

FIGURE 15. Turbulent Prandtl number and correlation coefficients.

4. Entrainment and preferential transport

As the experimental results for the average turbulent Prandtl number σ_t summarized in table 1 indicate, the turbulent Prandtl number is very different from unity. It is different for different flows and even varies from location to location for the same flow. Transport mechanisms have been proposed (Taylor 1932; Townsend 1956) to explain those differences. Recently, Fiedler (1973) suggested an ordinary gradient diffusion

mechanism for momentum in a plane turbulent mixing layer. To be consistent with this model, however, the shear correlation $\overline{uv}$ should receive its largest contribution from the small-scale region.

Both the distribution of $\overline{u\theta}$ and the correlation coefficient $R_{u\theta}$ are shown in figure 13. Excluding the tail of the jet, the correlation coefficient between u and θ is fairly constant across the jet and equal to 0·5. Both unconditioned and turbulent zone values of the corrected turbulent 'shear stress' and the lateral component of the turbulent heat transfer are plotted in figure 14. That the turbulent zone values are less than the conventional averages in the central region is merely due to the 'switching terms' relating the two being of a certain sign. Since the non-turbulent zone averages for the 'shear stress' and heat transfer were too small (about an order of magnitude less) to be measured accurately, they were assumed to be effectively zero. Distributions of $\overline{v\theta}$ and $\overline{uv}$ have similar shapes and reach their maximum values at approximately the same radial location. This suggests that the transport mechanisms for momentum and heat are perhaps not radically different. Mean velocity and temperature profiles presented earlier show the inflexion points to be roughly at $r/r_{\frac{1}{2}} = 1{\cdot}1$ whereas $\overline{uv}$ and $\overline{v\theta}$ reach a maximum at approximately $r/r_{\frac{1}{2}} = 0{\cdot}78$, thus demonstrating the weakness of a simple gradient-type transport mechanism for either momentum or heat.

The correlation coefficients R_{uv} and $R_{v\theta}$ are presented in figure 15. As can be seen, $R_{v\theta} > R_{uv}$, indicating that the turbulent motions are more efficient in transporting heat than in transporting momentum. This is in agreement with Corrsin & Uberoi's (1950) measurements. The actual shape of the curves is nevertheless quite different as a result of the considerable scatter in their measurements. The unusually large values of $R_{v\theta}$ near the tail are most probably a result of contamination of the temperature signal due to the velocity-sensing hot wire. As pointed out by Corrsin & Uberoi (1950), the turbulent Prandtl number σ_t, defined as the ratio of 'eddy diffusivities' for momentum and heat, does not have any fundamental physical basis; nevertheless it provides an empirical measure of the ratio of momentum to heat transfer. In terms of the various measured quantities it can be expressed as

$$\sigma_t = \frac{(\overline{uv}/\overline{U}_m^2)\,\partial(\overline{\Theta}/\overline{\Theta}_m)/\partial r}{(\overline{v\theta}/\overline{U}_m\,\overline{\Theta}_m)\,\partial(\overline{U}/\overline{U}_m)/\partial r}.$$

Its variation across the jet was computed from least-squares curves fitted to the data. In qualitative agreement with Hinze & Van der Hegge Zijnen's (1949) indirect measurements, which vary from 0·4 to 0·7, σ_t is not constant across the jet. In view of the inadequacy of a simple gradient-type transport mechanism to describe this flow, this should not be surprising.

To compare the sizes of the eddies responsible for the momentum and heat transport, filtered correlations $\overline{u_f v_f}$ and $\overline{v_f \theta_f}$ were measured. Since simultaneous signals for u, v and θ were available, this was done by using two identical wave analysers (HP 302A, bandwidth = 6 Hz) set at the same centre-frequencies. In order to make measurements at low frequencies, the tape recorder was played back 32 times faster. By definition, of course,

$$\overline{uv} = \int_0^\infty \overline{u_f v_f}\,df, \quad \overline{v\theta} = \int_0^\infty \overline{v_f \theta_f}\,df.$$

Since $\overline{uv}$ and $\overline{v\theta}$ measurements were made independently, the accuracy of the filtered correlation measurements could be checked from the above relations. The difference

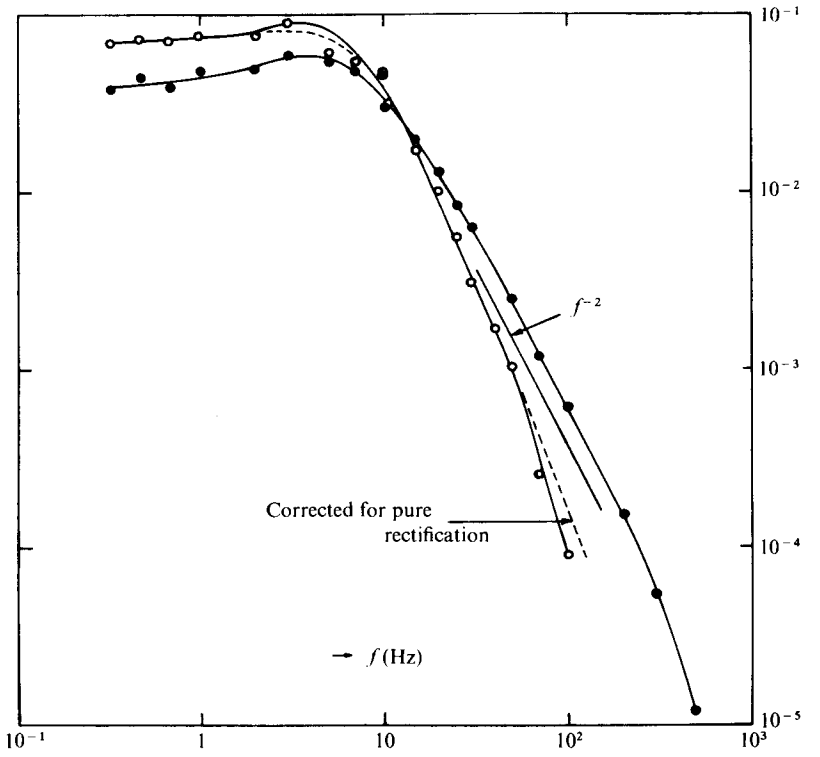

FIGURE 16. Filtered correlations at $r/r_{\frac{1}{2}} = 0{\cdot}8$.

$\circ, \overline{u_f v_f} \Big/ \int_0^\infty \overline{u_f v_f}\, df$; $\bullet, \overline{v_f \theta_f} \Big/ \int_0^\infty \overline{v_f \theta_f}\, df$.

(for both $\overline{uv}$ and $\overline{v\theta}$) was about 9%. Later these measurements were repeated with a single wave analyser using the identity

$$(u_f + v_f)^2 - (u_f - v_f)^2 = 4u_f v_f.$$

This method ensures that the centre-frequency is exactly the same. With this method, more scatter was noticed at high frequencies, otherwise the results were unchanged. For these measurements, shown in figure 16, as well as for the spectral density functions of u and θ, shown in figure 17, no attempt has been made to convert frequency to wave-number since on the one hand Taylor's hypothesis is not applicable for our case and on the other hand the proper convection velocity is strongly dependent on the wave-number (Wygnanski & Fiedler 1970).

From integration of the distributions in figure 16, $\overline{uv}$ gets about 70% of its value from contributions below 10 Hz (maximum burst rate) while $\overline{v\theta}$ gets about 50%. Although the bulk of the transport (for temperature as well as momentum) is accomplished by the large scales, the small scales are more efficient in transporting heat than in transporting momentum. Thus gradient-type diffusion is more important for heat than it is for momentum transport. Although this may look surprising at first, the physical reason for this can be ascribed to the fact that the length scale of temperature mixing is larger than that of momentum mixing. This is because while a scalar is conserved during fluid motion (in the absence of molecular diffusivity) momentum

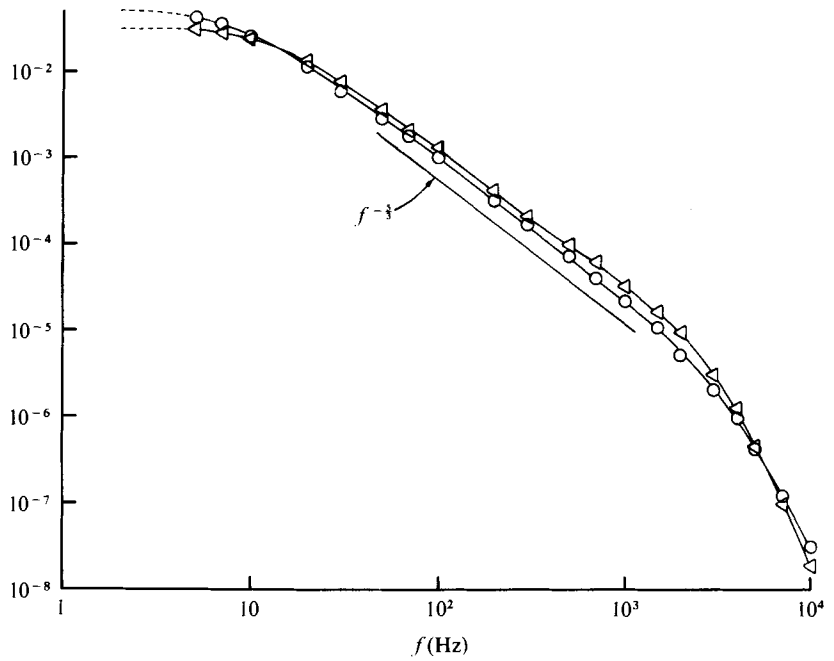

FIGURE 17. Spectral density of u and θ at jet centre-line. $x/D = 15$.

○, velocity, $E_{11}/\int_0^\infty E_{11}\,df$; ◁, temperature, $\Gamma/\int_0^\infty \Gamma df$.

is not, and, since the momentum of a fluid particle associated with these small-scale motions is continuously 'bleeding', the effective length is reduced.

$\overline{u_f v_f}$ drops sharply at 100 Hz, and, since $\overline{v_f \theta_f}$ does not show such behaviour, it was suspected that this strange cut-off for $\overline{u_f v_f}$ might be due to distortions in the velocity signals caused by high turbulence intensity. In order to investigate this effect on the $\overline{u_f v_f}$ spectrum, $u(t)$ and $\theta(t-\tau)$ signals at the centre-line were assumed to simulate undistorted u and v signals. A delay line was used to delay the temperature signal by an amount τ such that the correlation coefficient between $u(t)$ and $\theta(t-\tau)$ at the centre-line was the same as R_{uv} at $r/r_{\frac{1}{2}} = 0{\cdot}8$. The filtered correlation between these two signals was measured and served as the 'reference' (or true) spectrum. By analog means, these simulated signals were then distorted just as a cross-wire would distort them under conditions of pure rectification at $r/r_{\frac{1}{2}} = 0{\cdot}8$. Filtered correlations were measured again and compared with the 'reference' spectrum. The effect of pure rectification is seen to reduce the correlation $\overline{u_f v_f}$ algebraically; this correction is shown in figure 16.

In the absence of molecular conductivity (and consequently molecular viscosity), the conservation equation for temperature reduces to $D\Theta/Dt = 0$; indicating that the temperature of a fluid particle is indeed conserved during its motion. The only mechanisms responsible for the transport of heat (besides molecular diffusion) are then bulk convection and turbulent diffusion (or, more correctly, convection by all scales). If molecular viscosity is neglected, the momentum equation reduces to

$$D\mathbf{U}/Dt = -\rho^{-1}\nabla p.$$

Thus it is immediately apparent that the momentum of a fluid particle is not conserved during its motion, but is continuously changing. It is also clear that besides bulk convection and turbulent diffusion there is an additional mechanism for the momentum transport: pressure forces. At first, it could be expected that an additional mechanism for transport would make the velocity profile flatter than the temperature profile. Its effect, however, is just the opposite. Because of continuous 'bleeding' of momentum from a fluid particle due to pressure forces, the effective mixing length for momentum is less than that for heat. Within the turbulent region, therefore, the transport due to pressure forces is achieved at the expense of transport due to convection, thus resulting in an overall reduction in the net momentum transport. Momentum, as opposed to heat, can be imparted to fluid in the non-turbulent region through pressure forces across the interface. Since this results in the momentum being distributed over a larger fluid volume (assuming that there is no negative entrainment, heat cannot be transported across the turbulent/non-turbulent interface), this also makes the $\overline{U}_t$ profile steeper than the $\overline{\Theta}_t$ profile.

If we restrict our attention to scales which are small but which are large enough that 'bleeding' of momentum and heat due to molecular actions can be neglected, we can write down equations derived from the mixing length which give the heat flux and turbulent shear stress for individual length scales. This results in a range of frequencies where the filtered correlations behave as

$$\overline{u_f v_f} \sim f^{-2}, \quad \overline{v_f \theta_f} \sim f^{-2}. \tag{2}$$

Between 45 Hz and 250 Hz, which on the basis of the mean velocity would correspond to length scales between 3 cm and 17 cm (compared with the microscale $\lambda = 4{\cdot}96$ mm and Kolmogorov length $\eta = 0{\cdot}09$ mm), $\overline{v_f \theta_f}$ does indeed drop as f^{-2}.

This preferential transport of a scalar must nonetheless be viewed with the proper perspective, namely as resulting in a more uniform distribution of the scalar property than of the momentum within the flow field. It does not necessarily imply that relatively more scalar flux is transported laterally, nor does it imply, as shown by Jenkins & Goldschmidt (1976), that the scalar is transported much further into the ambient fluid. If the round jet is separated into two regions at the radial location where the heat flux and shear stress attain their maxima, all fluid elements in the central zone are losing both momentum and heat on average while fluid elements in the outer region are gaining momentum and heat. Since in a turbulent jet the longitudinal momentum and heat flux are constant at every section, we define

$$m = \tau_{\max}/(\text{total longitudinal momentum flux}),$$
$$h = q_{\max}/(\text{total longitudinal heat flux}).$$

Then the ratio m/h is a good measure of the relative transport of momentum and heat: from our measurements we get

$$m/h = 0{\cdot}94,$$

which is much higher than the turbulent Prandtl number of 0·61. If we consider the interfaces for velocity and temperature to be the same, the mass flow rate M_m which carries the momentum is

$$M_m = \int_0^\infty 2\pi r \rho \overline{U} dr,$$

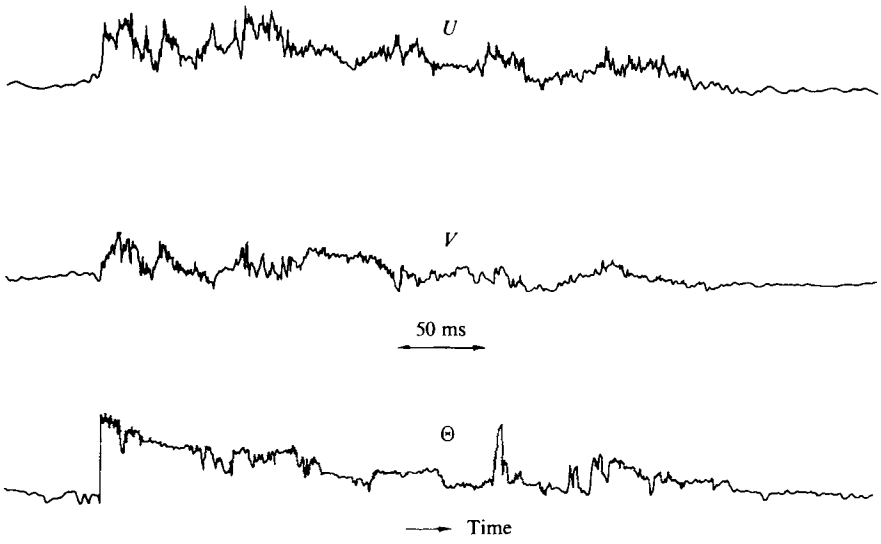

FIGURE 18. Simultaneous traces of U, V and Θ at $r/r_{\frac{1}{2}} = 1{\cdot}33$.

while the mass flow rate M_h which carries the heat is

$$M_h = \int_0^\infty 2\pi r \rho \overline{I(t)\, U} dr.$$

Since $I(t) \leqslant 1$, it is obvious that $M_h < M_m$. So, contrary to the implications of the turbulent Prandtl number, momentum is distributed over a larger fluid mass than heat; this also contributes to making the temperature profile relatively flatter.

Since the presence or absence of turbulence is independent of the magnitude of a passive scalar, there can be only one turbulent/non-turbulent interface, which we call the velocity interface. For the temperature, we shall take as the interface the boundary across which there is temperature variation, the fluid on one side being at the ambient temperature. Figure 18 shows simultaneous traces of U, V and Θ at one radial location in the jet. The difficulties in establishing the coincidence of temperature and velocity interfaces with absolute certainty are immediately apparent. Because of the contamination of the temperature signal (predominantly in regions of reserve flow) due to the influence of the velocity-sensing hot wire, there sometimes exist large temperature excursions in the non-turbulent regions. Although these can usually be identified as such (because of their peculiar shape), this is not always so, which makes the interface comparison difficult. As expected, the temperature signal shows a jump across the interface whereas the velocity signal is comparatively smooth. By studying a large number of simultaneous U and Θ traces we concluded that, within the present uncertainty inherent in our measurement technique, the temperature and velocity interfaces are coincident (Chevray & Tutu 1972).

Another question of interest is that raised by the non-zero value of the mean temperature in the non-turbulent region. The velocity sensitivity of the temperature-measuring wire (0·009 °C $(\mathrm{m/s})^{-1}$) is much too small to account for it. Improper detection is a possibility and to investigate it a 50 s (real time) chart recording was made at four radial positions. Direct measurements of the non-turbulent mean

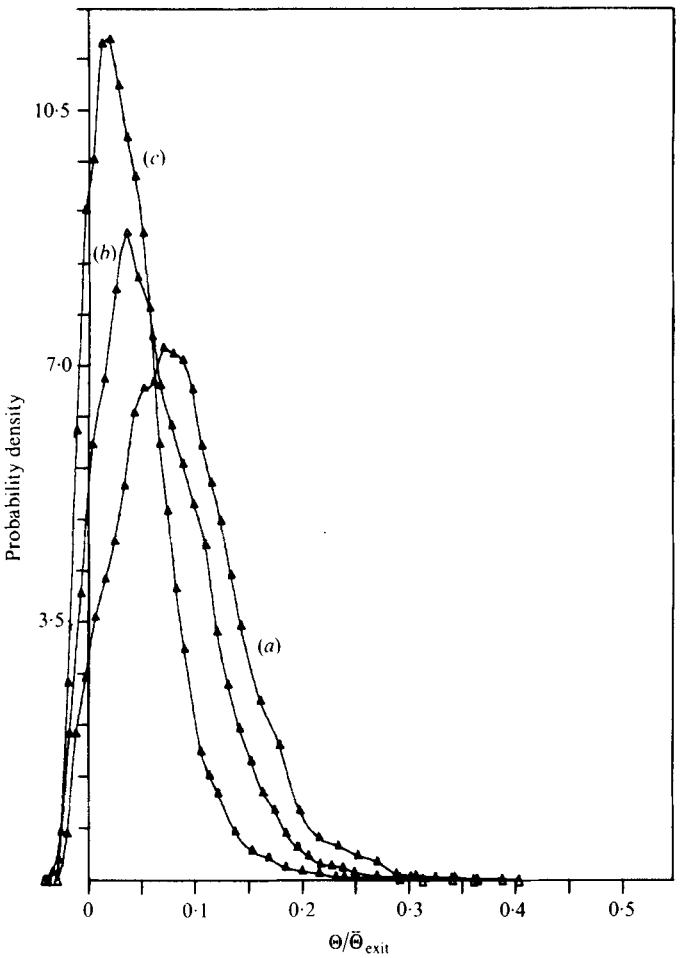

FIGURE 19. Probability density of temperature in non-turbulent zones. (*a*) $r/r_{\frac{1}{2}} = 0{\cdot}98$. (*b*) $r/r_{\frac{1}{2}} = 1{\cdot}33$. (*c*) $r/r_{\frac{1}{2}} = 1{\cdot}69$.

temperature, although not exactly the same as those obtained by analog measurements, were of the same order and showed the same trend, i.e. decreasing magnitude with increasing radius. Another explanation could be that there exists an ambient temperature gradient in the room owing to some hot air being recirculated. This would seem plausible were it not for the fact that the same trend is seen in all reported conditional measurements of temperature: see Kovasznay & Firasat Ali (1974, wake of a heated flat plate), Fiedler (1973, plane turbulent mixing layer), Jenkins & Goldschmidt (1976, two-dimensional plane jet) and Davies, Keffer & Baines (1975, plane turbulent jet). From this and similar studies, there is therefore no compelling argument at present which explains this anomalous temperature signal in the so-called 'non-turbulent zone'.

5. Conservation equations for conditioned variables and modelling

Although experimentalists developed conditional sampling techniques a long time ago (e.g. Kovasznay, Kibens & Blackwelder 1970; Kaplan & Laufer 1968) and demonstrated the important role that intermittency plays through the turbulent/non-turbulent interface, predictors have not made use of the analogous analytical techniques. In fact, only a few papers published recently by Libby (1975, 1976) and Dopazo (1978) make use of equations for the conditioned variables. Because the intermittency factor γ and the interface crossing rate $2f_\gamma$ enter naturally into such a description, it is to be expected that this approach will represent the physical phenomenon in more detail. Whereas Libby obtained a set of simultaneous equations for both the conventional unconditioned mean and the conditioned variables, we shall develop here the conservation equation for the intermittency function and the turbulent zone averages of the velocity components and temperature.

Let U, V and W be the instantaneous velocity components in the x, r and ϕ directions, respectively, in an axisymmetric intermittent turbulent flow. Then, following Libby (1975), we postulate the model equation for the intermittency function $I(t)$ as

$$\frac{DI}{Dt} = \frac{\partial I}{\partial t} + U\frac{\partial I}{\partial x} + V\frac{\partial I}{\partial r} + \frac{W}{r}\frac{\partial I}{\partial \phi} = \dot{s}, \tag{3}$$

where $\dot{s}$ is the creation term, i.e. the rate at which, following a fluid particle, I is created or destroyed. $\dot{s}$ is not quantitatively, however, the rate of creation of the turbulent fluid. They are related only in the sense that if no turbulent fluid is created $\dot{s} = 0$. Since $I(t)$ is everywhere zero in the non-turbulent region and unity in the turbulent region, it follows that the only instants when $\dot{s}$ can be non-zero are those when the interface is crossing the spatial position under consideration. It follows then that $\dot{s}$ is a train of pulses, one pulse occurring at each instant at which the interface passes through the given location. Assuming that in the turbulent shear flow under consideration the entrainment is positive at every instant and consequently the turbulent/non-turbulent interface always travels into the ambient irrotational fluid, it follows that DI/Dt and hence $\dot{s}$ are always positive. That is, each time the interface crosses a given location at a certain time t_i, a fluid particle in the non-turbulent region passes into the turbulent region. Since the interface is sharp, this results in a positive-going pulse for $\dot{s}$ at $t = t_i$. Because I changes from zero to unity during this fast process, we must have

$$\int_{t_i-\frac{1}{2}\Delta t}^{t_i+\frac{1}{2}\Delta t} (DI/Dt)\,dt = 1,$$

where Δt is an infinitesimal time element. So $\dot{s}$ can be written as a series of Dirac delta functions

$$\dot{s} = \delta(t-t_1) + \delta(t-t_2) + \ldots + \delta(t-t_i) + \ldots. \tag{4}$$

It is immediately apparent from (4) that $\dot{s}$ is independent of the speed with which the interface travels into the irrotational fluid, and hence independent of the rate of entrainment. Consequently, the average rate at which I is created is not proportional to the rate of creation of the turbulent fluid. Taking the average of (4) gives

$$\bar{\dot{s}} = 2f_\gamma. \tag{5}$$

Equations (4) and (5) are exact and require only that the instantaneous entrainment be positive at all times. Making use of the fact that even for a discontinuous function

$$\partial\overline{IQ}/\partial x_k = \overline{\partial(IQ)/\partial x_k} \quad \text{(see appendix)},$$

for a steady flow with $\tilde{\tilde{W}} = \tilde{\tilde{W}} = 0$ a time average of (3) yields

$$\overline{U}_t \frac{\partial\gamma}{\partial x} + \overline{V}_t \frac{\partial\gamma}{\partial r} + \overline{u_t \frac{\partial I}{\partial x}} + \overline{v_t \frac{\partial I}{\partial r}} + \frac{1}{r}\overline{w_t \frac{\partial I}{\partial \phi}} = 2f_\gamma, \tag{6}$$

where $\overline{U}_t$ and $\overline{V}_t$ are the turbulent zone averages of U and V, and u_t, v_t and w_t are the fluctuations above the turbulent zone averages. This, then, is the conservation equation for the intermittency factor γ; the last three terms on the left-hand side contribute only during interface crossings and will in general have to be modelled.

For an incompressible flow, the continuity equation in the cylindrical co-ordinate system is

$$\frac{\partial U}{\partial x} + \frac{\partial V}{\partial r} + \frac{1}{r}\frac{\partial W}{\partial \phi} + \frac{V}{r} = 0.$$

Multiplying this by $I(t)$ and taking the time average gives

$$\frac{\partial}{\partial x}(\gamma\overline{U}_t) + \frac{1}{r}\frac{\partial}{\partial r}(r\gamma\overline{V}_t) - 2f_\gamma = 0, \tag{7}$$

where use has been made of (3) and (5). Neglecting the viscous transport of momentum as usual, the momentum equations become

$$\frac{\partial U}{\partial t} + U\frac{\partial U}{\partial x} + V\frac{\partial U}{\partial r} + \frac{W}{r}\frac{\partial U}{\partial \phi} = -\frac{1}{\rho}\frac{\partial P}{\partial x}, \tag{8}$$

$$\frac{\partial V}{\partial t} + U\frac{\partial V}{\partial x} + V\frac{\partial V}{\partial r} + \frac{W}{r}\frac{\partial V}{\partial \phi} - \frac{W^2}{r} = -\frac{1}{\rho}\frac{\partial P}{\partial \phi}, \tag{9}$$

$$\frac{\partial W}{\partial t} + U\frac{\partial W}{\partial x} + V\frac{\partial W}{\partial r} + \frac{W}{r}\frac{\partial W}{\partial \phi} + \frac{VW}{r} = \frac{1}{\rho}\frac{1}{r}\frac{\partial P}{\partial \phi}. \tag{10}$$

Multiplying (8) by $I(t)$ and (3) by u_t, adding and averaging yields after some algebra

$$\gamma\overline{U}_t\frac{\partial\overline{U}_t}{\partial x} + \gamma\overline{V}_t\frac{\partial\overline{U}_t}{\partial x} + \frac{\partial}{\partial x}(\gamma\tilde{\tilde{u}}_t^2) + \frac{1}{r}\partial r(r\gamma\widetilde{u_t v_t})$$
$$= f_\gamma(\hat{U} + \check{U} - 2\overline{U}_t) - \frac{\gamma}{\rho}\frac{\partial\overline{P}}{\partial x} - \frac{1}{\rho}\overline{I\frac{\partial p}{\partial x}} = 0. \tag{11}$$

Similarly (9) and (10) give

$$\gamma\overline{U}_t\frac{\partial\overline{V}_t}{\partial x} + \gamma\overline{V}_t\frac{\partial\overline{V}_t}{\partial r} + \frac{\partial}{\partial x}(\gamma\widetilde{u_t v_t}) + \frac{1}{r}\frac{\partial}{\partial r}(r\gamma\tilde{\tilde{v}}_t^2) - \frac{\gamma}{r}\tilde{\tilde{w}}_t^2$$
$$= f_\gamma(\hat{V} + \check{V} - 2\overline{V}_t) - \frac{\gamma}{\rho}\frac{\partial\overline{P}}{\partial r} - \frac{1}{\rho}\overline{I\frac{\partial p}{\partial r}} = 0, \tag{12}$$

$$\frac{\partial}{\partial x}(\widetilde{u_t w_t}\gamma) + \frac{1}{r}\frac{\partial}{\partial r}(r\widetilde{v_t w_t}) + \frac{\gamma}{r}\widetilde{v_t w_t} = -\frac{1}{\rho r}\overline{I\frac{\partial p}{\partial \phi}}, \tag{13}$$

where $\overline{P}$ is the unconditioned average pressure and p is the fluctuation above it. Since $\widetilde{u_t w_t} = \widetilde{v_t w_t} = 0$ for an axisymmetric flow, (13) implies that $\overline{I\partial p/\partial\phi} = 0$. But $\overline{I\partial p/\partial x}$

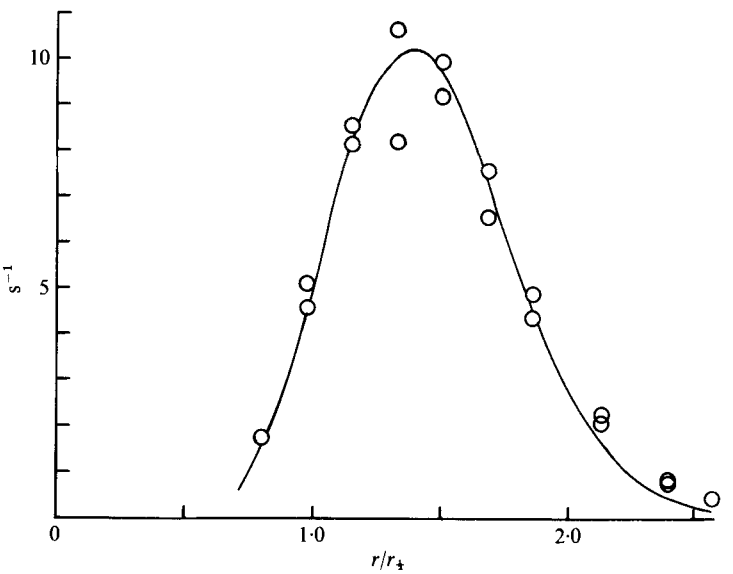

FIGURE 20. Modelling of f_γ. ——, $c_3\gamma(1-\gamma)\,\bar{J}_t/\Lambda$, $c_3 = 3{\cdot}447$, $\Lambda = r_{\frac{1}{2}}$; O, f_γ (direct measurement).

and $\overline{I\partial p/\partial r}$ should be of the same order as $\overline{I\partial p/\partial\phi}$, so it seems appropriate to neglect these terms. Neglecting the longitudinal mean pressure gradient and employing the boundary-layer approximations, (11) and (12) reduce to

$$\gamma\bar{U}_t\frac{\partial\bar{U}_t}{\partial x}+\gamma\bar{V}_t\frac{\partial\bar{U}_t}{\partial r}+\frac{1}{r}\frac{\partial}{\partial r}(r\gamma\widetilde{\overline{u_t v_t}})-f_\gamma(\hat{U}+\check{U}-2\bar{U}_t)=0, \tag{14}$$

$$\frac{1}{r}\frac{\partial}{\partial r}(r\gamma\widetilde{\overline{v_t^2}})-\frac{\gamma}{r}\widetilde{\overline{w_t^2}}=-\frac{\gamma}{\rho}\frac{\partial\bar{P}}{\partial r}. \tag{15}$$

Proceeding as above we can similarly find the equation to be satisfied by the turbulent zone-averaged temperature $\bar{\Theta}_t$ as

$$\gamma\bar{U}_t\frac{\partial\bar{\Theta}_t}{\partial x}+\gamma\bar{V}_t\frac{\partial\bar{\Theta}_t}{\partial r}+\frac{1}{r}\frac{\partial}{\partial r}(r\gamma\widetilde{\overline{v_t\theta_t}})-f_\gamma(\hat{\Theta}+\check{\Theta}-2\bar{\Theta}_t)=0. \tag{16}$$

Within a fully turbulent region ($\gamma\equiv 1, f_\gamma\equiv 0$), (14) and (16) reduce to the conventional Reynolds equations. In the intermittent region not only is the Reynolds-stress term modified but there appears an additional term which arises from a correlation of the type $\overline{\dot{s}u_t}$ and is therefore clearly related to the entrainment. To solve (6), (7) and (14) for $\bar{U}_t$, $\bar{V}_t$ and γ and (16) for $\bar{\Theta}_t$, we must model the rest of the terms.

If it is assumed that the interface is not folded on itself, i.e. that the instantaneous lateral co-ordinate of the interface at a given longitudinal location x is a single-valued function of r, then $-\partial\gamma/\partial r$ is the probability density function of the interface location. Then f_γ must clearly be proportional to it and from dimensional reasoning we can write

$$f_\gamma=-(c_1\bar{U}_m+c_2\bar{U}_t)\,\partial\gamma/\partial r. \tag{17}$$

Since no combination of the constants c_1 and c_2 could be found for which (17) represented the experimental results, it appears that our assumption regarding the

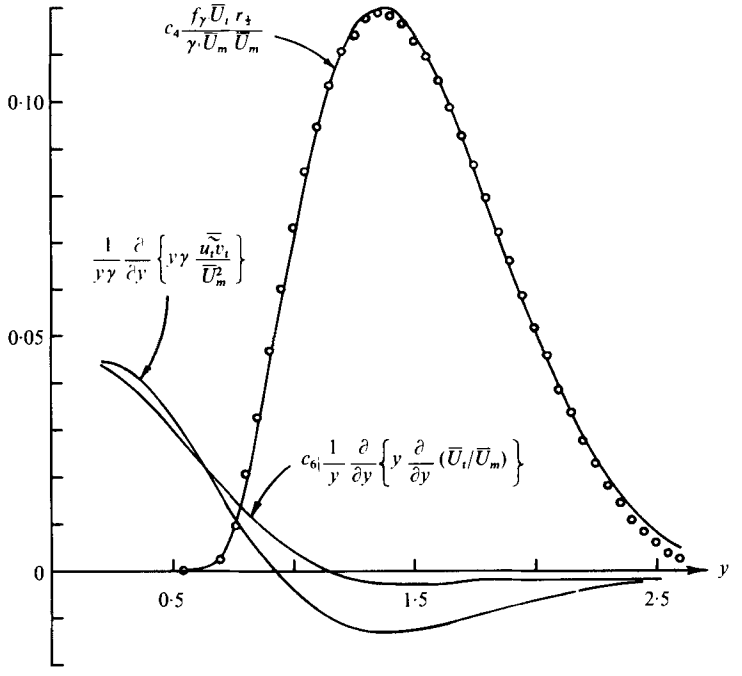

FIGURE 21. Modelling of modified Reynolds-stress and entrainment terms for momentum. $c_4 = 1{\cdot}011 \approx 1{\cdot}0$, $c_6 = 0{\cdot}0169$, $y = r/r_{\frac{1}{2}}$.

$$\circ, \frac{f_\gamma}{\gamma}(2\overline{U}_t - \hat{U} - \check{U})\frac{r_{\frac{1}{2}}}{\overline{U}_m^2}.$$

folding of the interface is a poor one. From the limiting values of f_γ as γ tends to 0 and 1, Libby has suggested

$$f_\gamma = c_3\gamma(1-\gamma)\overline{U}/\Lambda, \tag{18}$$

where we have now just one constant and where Λ is a length scale of the order of the width of the shear flow. As Libby has shown, (18) gives good agreement only in either the inner or outer region of the flow. Replacing $\overline{U}$ by the turbulent zone average, however, we obtain good results as shown in figure 20.

Whereas the dominant modified Reynolds-stress and heat-flux terms can be approximated in the usual manner without difficulty, the entrainment terms require separate treatment. One of the simplest closures representing these terms is

$$-f_\gamma(\hat{U} + \check{U} - 2\overline{U}_t) = c_4 f_\gamma \overline{U}_t, \tag{19}$$

$$-f_\gamma(\hat{\Theta} + \check{\Theta} - 2\overline{\Theta}_t) = c_5 f_\gamma \overline{\Theta}_t r_{\frac{1}{2}}/r. \tag{20}$$

For $\hat{U} \approx \check{U} \approx 0{\cdot}5\overline{U}_t$ as our measurements indicate, a value of $c_4 = 1{\cdot}01$ gives an excellent fit for the entrainment term as seen in figure 21. For (20), similar calculations were made with $c_5 = 1{\cdot}1$ and are presented in figure 22. Although the agreement is quite good in the inner part, this is not so for large values of r. This lack of agreement is not surprising since our measurements are unreliable in these regions owing to contamination of the temperature signal by the velocity-sensing wire.

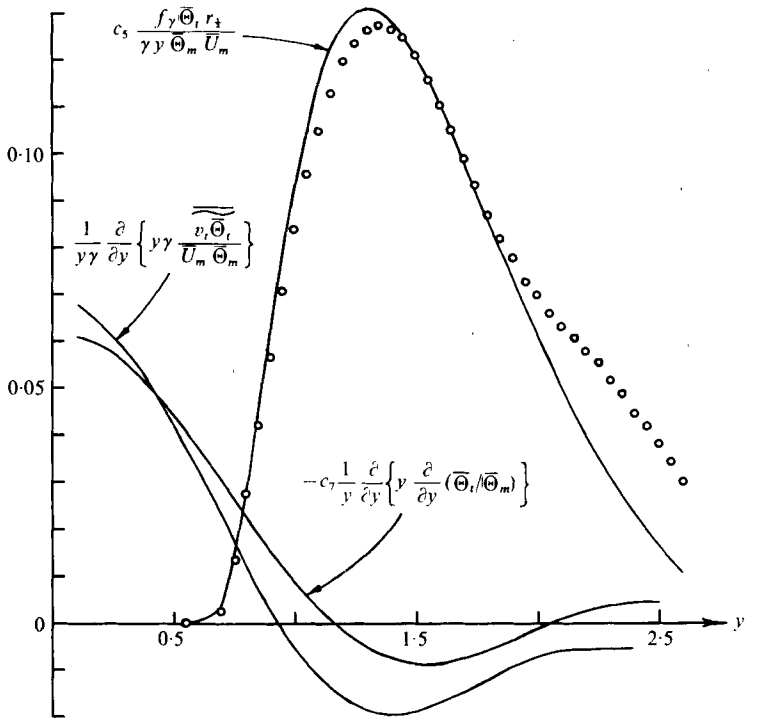

FIGURE 22. Modelling of modified heat-flux and entrainment terms for temperature. $c_5 = 1{\cdot}1$, $c_7 = 0{\cdot}0287$, $y = r/r_{\frac{1}{2}}$.

$$\circ, \frac{f_\gamma}{\gamma}(2\Theta_t - \hat{\Theta} - \check{\Theta})\frac{r_{\frac{1}{2}}}{\overline{U}_m \overline{\Theta}_m}.$$

6. Concluding remarks

Within the uncertainties in our measurement technique due to ambient temperature fluctuations, contamination of the temperature signal by the velocity-sensing hot wire in regions of reverse flow, etc., the velocity and temperature interfaces are coincident. There nevertheless exists a distinct possibility of occasional non-coincidence of the temperature and velocity interfaces on the basis of this and other previously published measurements in free turbulent shear flows.

From our conditional measurements, fluid particles in the turbulent zones are seen to move fast (compared with the mean velocity) and outwards, whereas fluid particles in the non-turbulent zones move slowly and inwards. Point measurements with respect to the interface suggest that jets of fluid are shot out periodically from the central regions, thus greatly increasing the surface undulations of the interface. The measurements also suggest that the interface has crevices in zones of high γ where rapid entrainment is taking place. Probability densities of the lengths of turbulent and non-turbulent durations indicate that the interface is a highly convoluted surface and that there is nothing like an average turbulent bulge.

The conventional turbulent Prandtl number is found to vary across the flow with a value of 0·61 at the location of maximum shear. Filtered correlation measurements show that large-scale turbulent motions are responsible for the bulk of momentum and heat transport, and also that small scales are more efficient in transporting heat

than in transporting momentum. Consequently, whereas bulk convection cannot be neglected for momentum transport, gradient-type diffusion cannot be neglected for heat transport if it is included for momentum transport.

Conservation equations for turbulent zone averages of the temperature, velocity and intermittency factor are derived and a model for some of the resulting terms is suggested. Under the assumption that the instantaneous entrainment is always positive, it is shown that $\dot{s}$, the average creation term in the equation for $I(t)$, is exactly equal to $2f_\gamma$. From these equations and on the basis of the present measurements, the entrainment terms dominate the terms of Reynolds-stress type in the outer regions of the jet.

Special thanks are due to E. E. O'Brien for his help in many capacities throughout this study. The financial support of the National Science Foundation under Grants GK30479 and KO40738 is gratefully acknowledged. Partial support from the Japan Society for the Promotion of Science (Gakujutsu shinkoo kyookai) while one of the authors (RC) was a Visiting Professor at the Universities of Hokkaido and Tokyo is gratefully acknowledged.

Appendix. Proof that $\overline{\partial(IQ)/\partial x_k} = \partial(\overline{IQ})/\partial x_k$

We assume an ergodic process

$$\overline{\frac{\partial}{\partial x_k}(IQ)} = \lim_{\substack{T\to\infty \\ \Delta t\to 0}} \frac{1}{T}\left(\int_{T_t}\frac{\partial(IQ)}{\partial x_k}dk + \int_{T_n}\frac{\partial(IQ)}{\partial x_k}dt + \sum_i \int_{t_i-\frac{1}{2}\Delta t}^{t_i+\frac{1}{2}\Delta t}\frac{\partial IQ}{\partial x_k}\,dt\right). \tag{A 1}$$

Here $Q(\mathbf{x}, t)$ is any property which is at least continuous in the turbulent and non-turbulent zones separately and T_t and T_n are the turbulent and non-turbulent durations, respectively. On the right-hand side of this equation, corresponding to non-turbulent regions, the second term is zero. Only terms of the first and third kind will be considered in detail. Let c_k be the instantaneous component of the interface convection velocity in the x_k direction, then consider one of the terms (say a trailing edge) with t_i the interface crossing time:

$$\int_{t_i-\frac{1}{2}\Delta t}^{t_i+\frac{1}{2}\Delta t}\frac{\partial(IQ)}{\partial x_k}dt = \frac{Q_{\text{t.s.}}}{c_k},$$

where t.s. refers to the turbulent side of the interface. (For a leading edge we should have similarly $-Q_{\text{t.s.}}/c_k$.) For N interface crossings, therefore,

$$\lim_{\substack{T\to\infty \\ N\to\infty}} \frac{\frac{1}{2}N}{T}\frac{1}{\frac{1}{2}N}\sum_{i=1}^{N}\int_{t_i-\frac{1}{2}\Delta t}^{t_i+\frac{1}{2}\Delta t}\frac{\partial(IQ)}{\partial x_k}dt = f_\gamma\left\{\left(\widehat{\frac{Q_{\text{t.s.}}}{c_k}}\right) - \left(\widecheck{\frac{Q_{\text{t.s.}}}{c_k}}\right)\right\}. \tag{A 2}$$

We also have

$$\frac{\partial}{\partial x_k}\overline{(QI)} = \lim_{T\to\infty}\frac{\partial}{\partial x_k}\frac{1}{T}\int_T (QI)\,dt = \lim_{\substack{T\to\infty \\ \Delta t\to 0}}\frac{1}{T}\frac{\partial}{\partial x_k}\int_{T_t} Q\,dt,$$

$$\frac{\partial}{\partial x_k}\int_{T_t} Q\,dt = \frac{\partial}{\partial x_k}\left(\int_{t_1+\frac{1}{2}\Delta t}^{t_2-\frac{1}{2}\Delta t} Q\,dt + \int_{t_3+\frac{1}{2}\Delta t}^{t_4-\frac{1}{2}\Delta t} Q\,dt + \ldots\right),$$

with t_{2n} the times corresponding to trailing edges and t_{2n+1} the times corresponding to leading edges. In addition,

$$\frac{\partial}{\partial x_k}\int_{T_i} Q\,dt = \left(\int_{t_1+\frac{1}{2}\Delta t}^{t_2-\frac{1}{2}\Delta t}\frac{\partial Q}{\partial x_k}dt + \int_{t_3+\frac{1}{2}\Delta t}^{t_4-\frac{1}{2}\Delta t}\frac{\partial Q}{\partial x_k}dt + \ldots\right)$$
$$+\left\{Q\left(t_2-\frac{\Delta t}{2}\right)\frac{\partial t_2}{\partial x_k} - Q\left(t_1+\frac{\Delta t}{2}\right)\frac{\partial t_1}{\partial x_k} + Q\left(t_4-\frac{\Delta t}{2}\right)\frac{\partial t_4}{\partial x_k}\right.$$
$$\left. - Q\left(t_3+\frac{\Delta t}{2}\right)\frac{\partial t_3}{\partial x_k} + \ldots\right\},$$

so that

$$\frac{\partial}{\partial x_k}(\overline{QI}) = \lim_{\substack{T\to\infty\\ N\to\infty}}\left\{\frac{1}{T}\left(\int_{T_i}\frac{\partial(IQ)}{\partial x_k}dt\right) + \frac{\frac{1}{2}N}{T}\frac{1}{\frac{1}{2}N}\left(Q_{\text{t.s.}}\frac{\partial t_2}{\partial x_k} - Q_{\text{t.s.}}\frac{\partial t_1}{\partial x_k} + \ldots\right)\right\}$$
$$= \lim_{\substack{T\to\infty\\ \Delta t\to 0}}\frac{1}{T}\int_{T_i}\frac{\partial(IQ)}{\partial x_k}dt + f_\gamma\left\{\overline{\left(\frac{Q_{\text{t.s.}}}{c_k}\right)} - \left(\frac{\overline{Q_{\text{t.s.}}}}{c_k}\right)\right\}.$$

For the case Q = constant, the second term on the right-hand side of these equations becomes

$$f_\gamma Q\left\{\overline{\left(\frac{1}{c_k}\right)} - \left(\frac{1}{c_k}\right)\right\} = Q\frac{\partial\gamma}{\partial x_k}.$$

Hence, at a given spatial position, we can expect a large difference between the leading- and trailing-edge convection velocities in the direction of the gradient of the intermittency factor. Combining (A 1)–(A 3), we obtain $\partial(\overline{IQ})/\partial x_k = \overline{\partial(IQ)/\partial x_k}$.

REFERENCES

Champagne, F. H. & Sleicher, C. A. 1967 *J. Fluid Mech.* **28**, 177.

Chevray, R. & Tutu, N. K. 1972 *Rev. Sci. Instrum.* **43**, 1417.

Corrsin, S. 1943 *N.A.C.A. Rep.* no. W-94.

Corrsin, S. 1949 *N.A.C.A. Tech. Note* no. 1864.

Corrsin, S. & Kistler, A. L. 1954 *N.A.C.A. Rep.* no. 1244.

Corrsin, S. & Uberoi, M. S. 1950 *N.A.C.A. Rep.* no. 998.

Davies, A. E., Keffer, J. F. & Baines, W. D. 1975 *Phys. Fluids* **18**, 770.

Dopazo, C. 1978 Submitted for publication.

Fiedler, H. E. 1973 *2nd IUTAM–IUGG Symp. Turbulent Diffusion in Environmental Pollution, Univ. Virginia.*

Fiedler, H. E. & Head, M. R. 1966 *J. Fluid Mech.* **25**, 719.

Hinze, J. O. & Van der Hegge Zijnen, B. G. 1949 *Appl. Sci. Res.* A **1**, 435–461.

Jenkins, P. E. & Goldschmidt, V. W. 1976 *Phys. Fluids* **19**, 613.

Kaplan, R. E. & Laufer, J. 1968 *Proc. 12th Int. Cong. Appl. Mech.* p. 236.

Kovasznay, L. S. G., Kibens, V. & Blackwelder, R. F. 1970 *J. Fluid Mech.* **41**, 283–325.

Kovasznay, L. S. G. & Firasat Ali, S. 1974 *Proc. 5th Int. Heat Transfer Conf., Tokyo*, vol. 2, p. 99.

Libby, P. A. 1975 *J. Fluid Mech.* **68**, 273.

Libby, P. A. 1976 *Phys. Fluids* **19**, 494.

Mayer, E. & Divorky, D. 1966 *A.I.A.A. J.* **4**, 1995.

Mobbs, F. R. 1968 *J. Fluid Mech.* **33**, 227.

Paizis, S. T. & Schwarz, W. H. 1974 *Rev. Sci. Instrum.* **45**, 348.

Phillips, O. M. 1972 *J. Fluid Mech.* **51**, 97.

SUNYACH, M. 1971 Thèse Dr-ès-Sc., Université de Lyon.
TAYLOR, G. I. 1932 *Proc. Roy. Soc.* A **135**, 685.
THOMAS, R. M. 1973 *J. Fluid Mech.* **57**, 549.
TOWNSEND, A. A. 1949 *Austr. J. Sci. Res.* A **2**, 451.
TOWNSEND, A. A. 1956 *The Structure of Turbulent Shear Flow.* Cambridge University Press.
TUTU, N. K. 1976 Ph.D. dissertation, State University of New York, Stony Brook.
TUTU, N. K. & CHEVRAY, R. 1975 *J. Fluid Mech.* **71**, 785.
TUTU, N. K. & CHEVRAY, R. 1976 *Rev. Sci. Instrum.* **47**, 163.
WYGNANSKI, I. & FIEDLER, H. 1969 *J. Fluid Mech.* **38**, 577.
WYGNANSKI, I. & FIEDLER, H. 1970 *J. Fluid Mech.* **41**, 327.